



Adaptive Controller of Bidirectional DC-DC Converter Based on Extreme Learning Machine for Electric Vehicle

Yusrizal Afif^{1*} Herlambang Setiadi¹ Muhammad Abdillah²

¹*Department of Advanced Technology, Faculty of Advanced Technology and Multidiscipline,
Universitas Airlangga, Surabaya, Indonesia*

²*Department of Electrical Engineering, Faculty of Industrial Technology, Universitas Pertamina,
Jakarta, Indonesia*

* Corresponding author's Email: yusrizal@ftmm.unair.ac.id

Abstract: This paper proposed a novel adaptive controller of a non-isolated bidirectional coupled inductor DC converter based on an extreme learning machine (ELM) for electric vehicles. MATLAB and SIMULINK are used as the software platform to simulate the proposed method. Different operating conditions are considered to show the efficacy of the extreme learning machine. From the simulation results, it is found that by designing the controller based on an extreme learning machine the controller can automatically adjust the value depending on the operating conditions (motor moving forward, backward, and regenerative braking). In addition, the performance of the motor with DC converter based on ELM is compared with DC converter based on grey wolf optimization and based on conventional PI controller. This is indicated by the overshoot and the settling time is much better when using controller based on an extreme learning machine (overshoot 221.6 and settling time 3.8 second).

Keywords: Bidirectional, Clean energy technology, DC converter, ELM, Electric vehicle.

1. Introduction

Global warming and energy security are the main issues in the modern era [1]. This issue came out due to the application of fossil fuels not only in the power system sector but also in the transportation sector [2]. Hence it is important to reduce the application of fossil fuels on the transportation sector, as this sector is one of the highest contributors to global warming and the greenhouse gas effect. One of the ways to reduce the application of fossil fuels in the transportation sector is by using electric vehicles [3].

The research effort in [4], shows the effect of electric vehicles on greenhouse gas emissions. It was found that by using electric vehicles the emissions on the transportation side can be reduced. The effect of electric vehicles on gas emissions in Europe is reported in [5]. From the study, it was found that by adding more electric vehicles in the transportation sector, the emissions in 29 European countries are reduced. Vilaca et al [6], show that the application of

electric vehicles can reduce the greenhouse gas effect significantly. From above study, it is found that electric vehicles bring positive impact of the society. One of the main issues of electric vehicles is what is the best electric motor that must be used. Recently direct current (DC) motor shows promising result when use as the electric vehicles motor [7].

The application of motor DC as electric vehicle motor is reported in [8]. From the simulation results, it is noticeable that DC motor could be used as the electric vehicle motor. In addition, by using DC motor the total cost can be reduced. Research effort in [9], shows that DC motor could provide satisfied power performance when used as the electric vehicle motor. Bahrami et al shows the efficacy of DC motor for electric vehicle when operated in regenerative braking operation as reported in [10]. However, the problem is motor DC is how to the control the speed of DC motor. Generally, motor DC speed can be controlled by changing the voltage input of the motor. To change the magnitude of DC voltage, DC to DC converter is essential [11].

The application of DC converter as electric vehicle drivetrains is reported in [12]. From the simulation results it is noticeable that DC converter is essential tools in the electric vehicle. Research effort in [13] shows the application of bidirectional DC converter for electric vehicle driver. It is noticeable that by using bidirectional DC converter the speed of electric vehicle can be controlled optimally. In addition, by using bidirectional DC converter, the regenerative braking mechanism can be carried out. The application of buck-boost converter as the driver of permanent magnet brushless DC motor is reported in [14]. It is reported from the results that bidirectional converter is one of the best drivers for electric vehicle. To control the voltage magnitude of DC converter, switching mechanism is playing important role. The design the switching mechanism optimally, the controller of the switching is essential. PI controller is common controller that usually used as the converter controller [15]. However, PI controller is out of date as now a lot of disturbance and non-linearity is affected in electric vehicle. Hence, designing the controller based on artificial intelligence is inevitable.

The application of artificial intelligence in power engineering is developed significantly over the past few years. Application of bat algorithm for designing power system stabilizer (PSS) is reported in [16]. From the simulation results it is found that by designing PSS based on the bat algorithm, the small signal stability of power system can be enhanced even though renewable energy power plant are added to the system. Research effort in [17], shows the application of grey wolf optimization (GWO) for designing PID controller. The PID controller is used as the controller of the DC-DC buck converter. From the simulation results it is noticeable that by using PID based on GWO, the PID controller can giving a better signal controller to the PWM to activate the converter switch. The comparison of different algorithm for designing PID controller of DC-DC boost converter is reported in [18]. GWO, particle swarm optimization (PSO) and genetic algorithm is considered in [18]. It is reported that three different algorithms proposed in [18] can be used to tune the PID controller parameter. However, the best performance is showed by the PID based on GWO. Although optimization-based algorithm can be used to design the PID controller of DC-DC converter. They have disadvantages in term of adaptiveness. When there is different operating condition, optimization-based algorithm cannot automatically update the PID controller parameter. They will always start the optimization again every time the operating conditions is changing. Hence, it will take

a lot of time for the converter to adjust the switching as the optimization process need several minutes to find the optimal parameter. Hence, it is important to make the PID controller adaptive to any wide range operating condition.

Amount numerous types of artificial intelligence for making controller become adaptive, machine learning is attracting more engineers to apply the concept to solve engineering problems. As reported in [19], extreme learning machine can be used to monitor the performance of power system. From the results it is noticeable that extreme learning machine can detect any condition of power system over the wide range operation condition. Hence, this paper proposed the application of extreme learning machine to make the PI controller adaptive to any changing of the operating condition. This adaptive PI controller is used as the controller of DC-DC bidirectional converter. The converter is used as the driver of electric vehicle. The rest of the paper is organized as follows: section 2 shows the fundamental theory of the paper. The method of designing proposed controller is presented in section 3. Result and discussion are presented in section 4. Section 5 highlighted the contribution and the future study.

2. Modelling

2.1 Modelling of DC-DC boost converter

The DC/DC boost converter increases the output voltage from a certain input voltage level by controlling the “ON” and “OFF” duration of the power switch. The averaged state space equation of DC/DC boost converter over one period is obtained by combining the dynamic equations during “ON” and “OFF” states. The complete state equation of DC/DC boost converter as given in Eqs. (1) and (2) [20].

$$\begin{bmatrix} \dot{x}_1 \\ \dot{x}_2 \end{bmatrix} = \begin{bmatrix} -\frac{R_s}{L} & -\frac{s_1(t)}{L} \\ \frac{s_2(t)}{C} & -\frac{1}{CR_L} \end{bmatrix} \begin{bmatrix} x_1 \\ x_2 \end{bmatrix} + \begin{bmatrix} \frac{1}{L} \\ 0 \end{bmatrix} u \quad (1)$$

$$y = [0 \quad 1] \begin{bmatrix} x_1 \\ x_2 \end{bmatrix} \quad (2)$$

Where R_s and L are the inductance and resistance of the boost converter. While C and R_L are the capacities and resistance in the load side. In addition, x_1 and x_2 are representation of current and voltage of the converter [20]. Fig. 1 shows the electrical circuits of DC-DC boost converter.

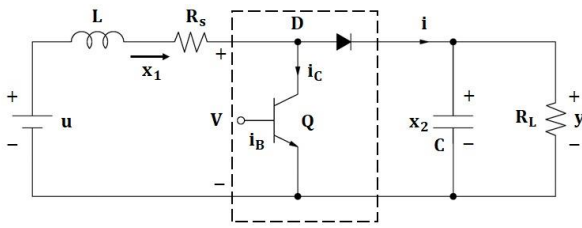


Figure. 1 Electrical circuits of DC-DC boost converter

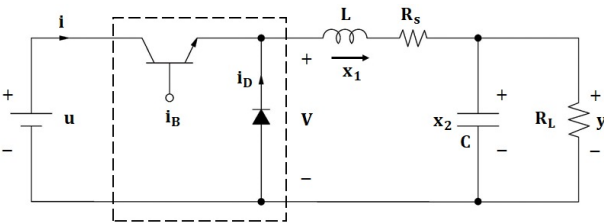


Figure. 2 Electrical circuits of DC-DC buck converter

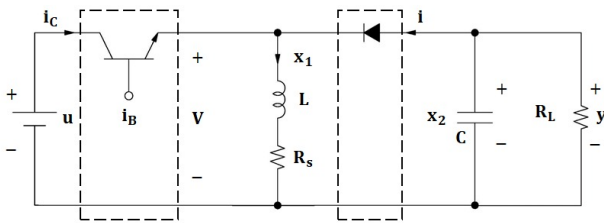


Figure. 3 Electrical circuits of DC-DC buck-boost converter

2.2 Modelling of DC-DC buck converter

The DC-DC buck converter is producing an output that lower than the voltage source. To analysing the buck converter, it also essential to investigate the steady state conditions. The mathematical representation of DC/DC buck converter is described in Eqs. (3) and (4) [20].

$$\begin{bmatrix} \dot{x}_1 \\ \dot{x}_2 \end{bmatrix} = \begin{bmatrix} -\frac{R_s}{L} & -\frac{1}{L} \\ \frac{1}{C} & -\frac{1}{CR_L} \end{bmatrix} \begin{bmatrix} x_l \\ x_l \end{bmatrix} + \begin{bmatrix} \frac{s_3(t)}{L} \\ 0 \end{bmatrix} u \quad (3)$$

$$y = [0 \quad 1] \begin{bmatrix} x_l \\ x_l \end{bmatrix} \quad (4)$$

Where R_s and L are the inductance and resistance of the buck converter. While C and R_L are the capacities and resistance in the load side. In addition, x_1 and x_2 are representation of current and voltage of the converter [20]. Fig. 2 shows the electrical circuits of DC-DC buck converter.

2.3 Modelling of DC-DC buck-boost converter

A converter that operated in both directions is needed for more specialized applications such as in electric vehicles. The application of a bidirectional converter will make the EV operated optimally. The

basic scheme of a bidirectional non isolated converter circuit is the same as a boost converter and a buck converter. The difference is on how to control the switch so that the converter can operated either in boost or buck converter. The switch used in this converter is IGBT type. The IGBT switch is in parallel with the diode. Parallel diodes aim to make the converter work bidirectional when the boost mode and buck mode are the same. Fig. 3 shows the electrical circuits of DC-DC buck-boost converter.

In EV, the low-voltage side component is a battery in parallel with a capacitor. This capacitor aims to regulate the voltage ripple when the bidirectional converter works in buck mode. The high-voltage side component is a motor which is also paralleled with a capacitor. The capacitor on this side is used to regulate the voltage ripple when the bidirectional converter is working in boost mode. The choice of inductor greatly affects the ability of the converter to operate. The mathematical representation of buck-boost converter is described in Eqs. (5) and (6) [20].

$$\begin{bmatrix} \dot{x}_1 \\ \dot{x}_2 \end{bmatrix} = \begin{bmatrix} -\frac{R_s}{L} & -\frac{s_2(t)}{L} \\ \frac{s_1(t)}{C} & -\frac{1}{CR_L} \end{bmatrix} \begin{bmatrix} x_l \\ x_l \end{bmatrix} + \begin{bmatrix} \frac{s_3(t)}{L} \\ 0 \end{bmatrix} u \quad (5)$$

$$y = [0 \quad 1] \begin{bmatrix} x_l \\ x_l \end{bmatrix} \quad (6)$$

3. Method

3.1 System configuration

In this research, lead acid battery is used as the source of the system. In each pack, the minimal voltage and capacity of lead acid batteries are 12 volt and 33 Ah. Six batteries are installed series, while the other five are installed parallel. Hence the total nominal voltage and the capacity is 72 volt and 165 Ah. The electric vehicle is represented by DC motor with an output power of 50 HP or 37.3 kW and voltage rating is 240 volt [21]. Non isolated bidirectional DC converter is used to adjust the battery output before sending it to the electric motor. When the electric vehicle is operated to move forward and backward the voltage input of motor is set it to 240 V. Regenerative braking is also considered in this research. To operate in regenerative braking condition the voltage is set to have 72 V

Adjustment of the output voltage value on the converter is carried out by changing the duty cycle value of the switch contained in the converter. The

Tabel 1. Parameter motor DC

Parameter	Value
Output Power	50 HP
Speed Rating	1750 RPM or 183.26 rad/s
Voltage Rating	240 V
Armature Resistance	0.1113 Ω
Armature Inductance	0.001558 H
Field Resistance	84.91 Ω
Field Inductance	13.39 H
Field-Armature Mutual Inductance	0.3406 H
Total Inertia	0.2053 kg.m ²
Viscous Friction Coefficient	0.007032 N.m.s
Coulomb Friction Torque	5.282 N.m

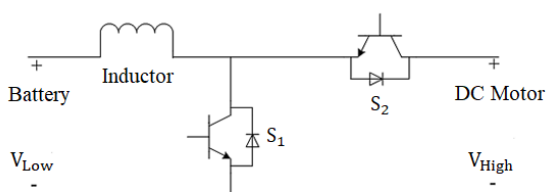


Figure. 4 Schematic diagram of the converter

duty cycle value is obtained from the calculation of the converter gain required by the system. The inductance selection of the inductor (in this case the coupled inductor) in the converter design must be appropriate. The inductance value of the inductor will affect the system by operate in continue conduction mode (CCM) or discontinue conduction mode (DCM). The inductor value also affects the current ripple in the system. The addition of an *L* filter on the battery side is carried out to smooth the battery current output before entering the coupled inductor circuit. Another important component selection is the capacitor. Capacitors is used to refine the voltage value on the high-voltage and low-voltage bus systems. Capacitors are installed in parallel on the two bus systems.

The load on the motor is a torque whose value can be changed. The value and shape of the torque characteristics in MATLAB are generated by the signal block builder. The motor must be able to maintain speed even if the load torque value is changed, except in regenerative braking mode. The speed in regenerative braking mode will decrease because it is part of the deceleration process. In addition, the load torque will also be negative. The system modeling is adjusted to the characteristics of the electric vehicle when operating acceleration and deceleration constant speed. The actual speed of the motor is used as feedback of the PI controller. However, the actual speed signal of the motor is first

converted into voltage units. Assuming the motor voltage is linear with the motor angular speed, the following equation is obtained

$$V = \frac{240}{183.26} \omega \tag{7}$$

Where *V* is actual voltage and ω is actual speed. The converted reference voltage and actual speed is compared to produce an error value. The error will then be used as input to the PI controller. At the rated speed of the motor, the PI controller will try to produce a DC signal output of ± 0.53846 . This value will be used to cut the carrier signal in the form of a saw signal with an amplitude of 1, so that a duty cycle of 53.846% will be generated. The error correction process will continue even though the error value is very small or 0, this condition is called the steady state condition. The PI output signal will be used as a trigger for the IGBT switch.

The separate amplified DC motor used in this study is the default of the DC machine block contained in the MATLAB software. Table 1 shows the motor parameters.

3.2 Non-isolated bidirectional DC converter modelling

Non-isolated bidirectional DC converter, can operate in two different directions. Boost mode occurs when the motor requires supply from the battery, it is assumed when the electric vehicle starts to move. While the buck mode occurs when the motor turns into a generator with a short time and supplies power to the battery. The modeling of a non-isolated bidirectional DC converter circuit without a coupled inductor and with a coupled inductor is shown in the following figure [22].

In Fig. 4 switch *S1* is the main switch when the converter operates in boost mode, while switch *S2* is an additional switch. Switch *S2* can be completely extinguished or operated with the trigger signal being the opposite of the trigger signal for switch *S1*. In buck mode, switch *S2* is the main switch, while switch *S1* is an additional switch. Switch *S1* can be completely extinguished or operated with the trigger signal being the opposite of the trigger signal for switch *S2*

In Fig. 5 switches *S1* and *S2* are the main switches when the converter operates in boost mode, while switch *S3* is an additional switch. Switch *S3* can be completely extinguished or operated with the trigger signal being the reverse of the trigger signal for switches *S1* and *S2*. In buck mode, switch *S3* is the main switch, while switches *S1* and *S2* are additional

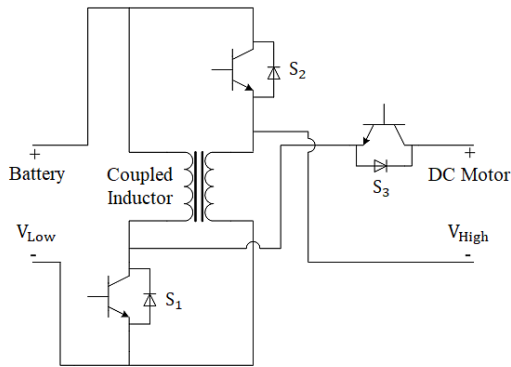


Figure. 5 Schematic diagram of the converter with coupled inductor

switches. Switches $S1$ and $S2$ can be completely extinguished or operated with the trigger signal being the opposite of the trigger signal for switch $S3$. This research uses the second operation, which is by using the reverse signal for the trigger signal on the additional switch in each mode.

The gain value in the converter can be increased by increasing the duty cycle value of the switch. However, the allowed duty cycle of each switch has certain limitations. This limit is used so that each switch does not experience excessive voltage stress. Voltage stress is a natural thing for a component if it operates to saturation conditions. The stress of each switch must be maintained so that it does not reach the saturation condition. If the stress reaches the saturation value, it will result in a decrease in the switch's ability to operate. Voltage stress is closely related to the switching frequency used. The greater the frequency value, the smoother the output voltage and current, but these conditions are contrary to what occurs in the switch. The switch will work with extra capabilities when using high frequencies (above 20 kHz), because the time during transients is getting shorter [23].

The addition of a coupled inductor in a non-isolated bidirectional DC converter can reduce the value of the duty cycle of each switch, so that the risk of saturation conditions is reduced. The gain ratio and duty cycle during boost mode and buck mode on a non-isolated bidirectional DC converter without a coupled inductor can be written as follows:

- Mode boost

$$Gain = \frac{V_{High}}{V_{Low}} = \frac{1}{1-D} \quad (8)$$

$$D = 1 - \frac{V_{Low}}{V_{High}} = 0.7 \quad (9)$$

- Mode buck

$$Gain = \frac{V_{Low}}{V_{High}} = D \quad (10)$$

$$D = \frac{V_{Low}}{V_{High}} = 0.3 \quad (11)$$

While the gain ratio during boost mode and buck mode on a non-isolated bidirectional DC converter with a coupled inductor can be written as follows:

- Mode boost

$$Gain = \frac{V_{High}}{V_{Low}} = \frac{1+D}{1-D} \quad (13)$$

$$D = \frac{V_{High}-V_{Low}}{V_{High}+V_{Low}} = 0.53846 \quad (14)$$

- Mode buck

$$Gain = \frac{V_{Low}}{V_{High}} = \frac{D}{2-D} \quad (15)$$

$$D = \frac{2 \cdot V_{Low}}{V_{High}+V_{Low}} = 0.46154 \quad (16)$$

Based on the comparison between Eqs. (9) and (14) in the boost mode and the comparison between Eqs. (11) and (16) in the buck mode, there is a difference in the value of the duty cycle when a coupled inductor is added to the circuit. The value of the IGBT switch voltage when using a bidirectional converter without a coupled inductor can be formulated as follows:

$$V_{S1} = V_{S2} = V_{High} \quad (17)$$

Meanwhile, when using a coupled inductor, it is formulated as follows.

$$V_{S1} = V_{S2} = \frac{V_{High}+V_{Low}}{2} \quad (18)$$

$$V_{S3} = V_{High} + V_{Low} \quad (19)$$

By substituting the value of the circuit parameter into the formula, the inductor value will be obtained. The values to be substituted are $I = 5$ A, $T = 1/10000$ s and $V_{Low} = 72$ V. Referring to the formula,

$$L = \frac{V_{Low} \cdot D \cdot T}{\Delta iL} = \frac{V_{Low} \cdot D}{\Delta iL \cdot f} \quad (20)$$

$$L = \frac{(72)(0.7)}{(5)(10.000)} \quad (21)$$

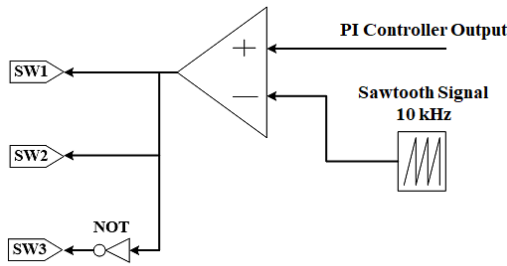


Figure. 6 Schematic diagram of PWM

Tabel 2. Parameter DC converter

Parameter	Nilai
Low Voltage Side Capacitor	$15 \times 10^{-3} \text{ F}$
High Voltage Side Capacitor	$15 \times 10^{-3} \text{ F}$
Coupled Inductor	1.1 Mh
Joint Inductance Coupled Inductor	1 mH
L . filter	0.01 mH
Coupled Inductor Resistance	1.1 pΩ
Coupled Inductor Joint Resistance	1 pΩ
Coupling Coefficient	0.9
Frequency	10 kHz

Tabel 3. Parameter of lead acid battery

Parameter	Nilai
Nominal Voltage	12 V
Rated Capacity (20 hour rate)	33Ah
Internal Resistance	7 mΩ
Initial Current for Charge	13.2 A or smaller
Control Voltage for Charge	14.5 V to 14.9 V
Approx. Mass	12 kg

Tabel 4. Parameter of lead acid battery in MATLAB

Parameter	Nilai
Nominal Voltage	72 V
Rated Capacity	165 Ah
Initial State-Of-Charge	85 %
Full Charge Voltage	109.167 %
Nominal Discharge Current	8.25 %
Internal Resistance	0.0084 Ω
Capacity @Nominal Voltage	100 %
Exponential Zone	[102.5 % 0.0833 %]

$$L = 1.008 \times 10^{-3} \text{ H} \quad (22)$$

$$L \approx 1.1 \times 10^{-3} \text{ H} \quad (23)$$

The coupling coefficient on the coupled inductor is quite high, namely 0.9. The author assumes the coupled inductor has a strong magnetizing effect between the two inductors. The resistance and mutual resistance of the coupled inductor are designed so small that it is assumed that the coupled inductor is a

pure inductor. The resistance value used is 1.1×10^{-9} ohms while the resistance value along with the coupling coefficient of 0.9 is 1×10^{-9} ohms. The capacitor capacitance selection is based on the capacitor calculation formula in the boost converter. The formula can be written as follows:

$$C_{min} = \frac{D}{R \cdot \Delta V / \Delta t \cdot f} \quad (24)$$

Where C_{min} , R , $\Delta V / \Delta t$, and f are the minimum capacity of capacitor (Farad), load resistance (ohm), voltage ripple (%) and switching frequency (Hz). The parameter values to be substituted are $R = 1.544$ ohms, $V / \Delta t = 1\%$ and $f = 10,000$ Hz. By substituting equation (10) with Eq. (24) and other parameter values, then,

$$C_{min} = \frac{0.7}{(1.544)(0.01)10,000} \quad (25)$$

$$C_{min} = 4.54 \times 10^{-3} \text{ F} \quad (26)$$

In the design of this capacitor the value of C taken is 330% of C_{min} . Hence, the capacitance of the capacitor used,

$$C_{min} = 15 \times 10^{-3} \text{ F} \quad (27)$$

In this paper the switching method is using pulse width modulation (PWM) as shown in Fig. 6. The PWM method compares the DC reference signal with the carrier signal in the form of a saw signal on the comparator. The frequency used in the carrier signal is 10kHz. The comparator output will be a discrete number between 0 and 1, with different on and off times according to the resulting duty cycle. PWM modeling is described as follows.

Overall, the parameters used in the non-isolated bidirectional DC converter with coupled inductor are based on the calculation of the non-isolated bidirectional DC converter without the coupled inductor. Parameters of all components used in non-isolated bidirectional DC converter with coupled inductor can be seen in Table 2.

3.3. Lead acid battery modelling

The lead acid battery used was manufactured by PANASONIC, based in Secaucus, New Jersey, USA. The lead acid battery used in this study was of the type LC-R1233P with a capacity of 33Ah and a nominal voltage of 12 V [21, 24]. The datasheet of the battery used is shown in Table 3.

The lead acid battery parameters are then

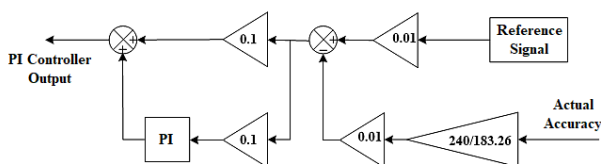


Figure. 7 Block diagram of speed controller

converted so that they can be input for parameter values in the MATLAB software. The lead acid battery parameters in MATLAB are shown in Table 4. Parameters in MATLAB, using battery parameters in series 6 and in parallel 5.

3.4. Speed controller

In speed regulation, the reference signal used is obtained from a constant DC signal with a certain value. The reference signal used is a voltage signal. The actual speed of the DC motor is censored first by using the gain block whose contents are Eq. (1). So when compared the two signals have the same units. Before being compared in block summary 1, the two signals enter the gain block again to reduce the signal amplitude value.

The goal is to make it easier for the PI controller to process data because the resulting error value has a smaller range. The comparison error is then forwarded to two different paths. The first path passes through the gain block and enters the summary block 2. While the second path passes through the gain block and the PI controller block, then enters the summary block 2. In summary 2 block, the two signal amplitude values are added up. The output of the block will be used as a DC reference signal for the comparator. Speed regulation modeling can be seen in Fig. 7.

3.5. Extreme learning machine

Extreme learning machine (ELM) has become popular in recent years to overcome various engineering and other fields problems since it was introduced by G. B. Huang in 2006. ELM structure is constructed by single hidden layer feed-forward network (SLFN). The ELM method is created to overcome the weakness in the SLFN, especially in the terms of the learning process. The parameters of ELM in its hidden layer are chosen randomly and do not have to be tuned. Furthermore, it can produce good generalizations. Thus, the process of making correlation between output and input data is extraordinary fast in this algorithm compared to the traditional learning algorithms such as SLFN. In addition, the hidden nodes could be set up before the

training samples are gained. There are two reasons why SLFN has low speed learning process [25]:

1. The application of gradient-based learning algorithm to carry out the training process.
2. Parameters on the net are determined via iteration using this learning method.

Conventional gradient-based learning algorithm method in the learning process such as back propagation or Levenberg Marquart and others with parameter on SLFN is determined manually. These parameters are the input weight and hidden bias which are also interconnected from one layer to another, so that it requires a slow learning speed process and it is often trapped in the local minima.

The formulation for the output function of ELM for generalized SLFN is defined as follows [25]:

$$y_L(\mathbf{x}) = \sum_{i=1}^L \varphi_i \psi_i(\mathbf{x}) = \Psi(\mathbf{x})\boldsymbol{\varphi} \quad (28)$$

where $\boldsymbol{\varphi} = [\varphi_1, \dots, \varphi_L]^T$ is vector of output weight between hidden layer of L nodes and the output node. $\boldsymbol{\psi}(\mathbf{x}) = [\psi_1(\mathbf{x}), \dots, \psi_L(\mathbf{x})]$ is the output vector of the hidden layer with respect to the \mathbf{x} . Input data of ELM in d -dimensional is mapped by $\boldsymbol{\psi}(\mathbf{x})$ to L -dimensional hidden-layer feature space \mathbf{H} [26].

In terms of learning process, ELM algorithm has difference with traditional learning algorithm where ELM goal is to reach not only the smallest error value but also the smallest norm of output weights at the same time as described in Eq. (29) [26].

$$\text{minimize: } \|\mathbf{H}\boldsymbol{\varphi} - \mathbf{T}\|^2, \|\boldsymbol{\varphi}\| \quad (29)$$

where \mathbf{H} is the hidden-layer output matrix.

$$\mathbf{H} = \begin{bmatrix} \boldsymbol{\psi}(\mathbf{x}_1) \\ \vdots \\ \boldsymbol{\psi}(\mathbf{x}_N) \end{bmatrix} = \begin{bmatrix} \psi_1(\mathbf{x}_1) & \dots & \psi_L(\mathbf{x}_1) \\ \vdots & \vdots & \vdots \\ \psi_1(\mathbf{x}_N) & \dots & \psi_L(\mathbf{x}_N) \end{bmatrix} \quad (30)$$

Using karush-kuhn tucker (KKT) optimality conditions, the least squares problem can be solved by Eq. (31) [27].

$$\boldsymbol{\varphi} = \mathbf{H}^T \left(\frac{I}{\lambda_r} + \mathbf{H}\mathbf{H}^T \right)^{-1} \mathbf{T} \quad (31)$$

where I , \mathbf{T} , and λ_r are identity matrix, target matrix, and regularization factor, respectively. $\mathbf{T} = [t_1, \dots, t_N]^T$.

By substituting Eq. (31) into Eq. (28), the output of ELM can be obtained as defined in the following equation [27]:

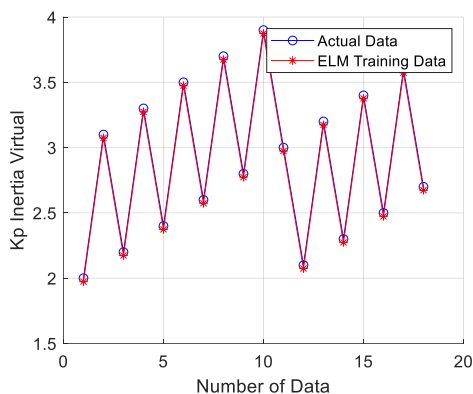


Figure. 8 Comparison of actual K_p value and K_p based on ELM

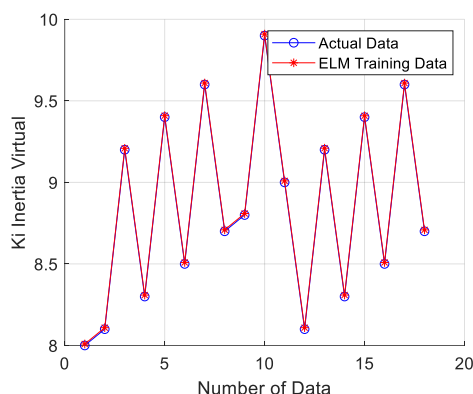


Figure. 9 Comparison of actual K_i value and K_i based on ELM

$$y(x) = \psi(x)H^T \left(\frac{I}{\lambda_r} + HH^T \right)^{-1} T \quad (32)$$

3.6 Procedure of designing the controller

This section focused on how ELM is implemented to PI controller, so the PI controller is adaptive again different operating condition of the electric vehicle. The input data for this training is speed reference and disturbance of the electric vehicle. In addition, the output is predicted parameter of PI controller (K_p and K_i). The procedure of adaptive PI includes the following steps [28]:

- Step 1. Conduct the training process using Eq (11)
- Step 2. Compute the accurateness of the predicted parameter using mean absolute error using Eq. (33)

$$MSE = \sum_{i=1}^N \frac{(\tilde{y}_i - y_i)^2}{N} \quad (33)$$

where \tilde{y}_i is predicted data yielded by proposed learning algorithm, while y_i is actual data. N is number of datasets utilized in training phase.

- Step 3. If the MSE value is minimum, print out the results. Otherwise go to the step 1 until the minimum MSE are obtained [28].

4. Results and discussions

This section focused on the showing the results of the proposed method. In addition, the discussion of the efficacy of the proposed method is also carried out in this section. All the simulation are carried out using MATLAB/SIMULINK environment. To simulated more realistic condition of the system all the modelling of bidirectional converter, DC motor and the associated controller are carried out using Simscape electrical library in SIMULINK MATLAB. While the ELM is coded using M-FILE in MATLAB. Three different case studies are carried out to shows the efficacy of the proposed method.

4.1 Training phase

The first step for investigating the performance of extreme learning machine by testing the algorithm with several data. In this paper the PI controller parameter of bidirectional converter is trained using ELM. Eighteen different operating is considered in the ELM training phase. The input of the ELM is the speed reference of motor DC and load torque reference from the motor DC. The output of the ELM training phase is the trained parameter of PI controller. Fig. 8 shows the comparison between actual K_p controller and the K_p based ELM. While Fig. 9 depicts the comparison of K_i actual, and K_i based ELM. It is noticeable that for ELM can mimic the value of conventional PI controller.

The execution time of ELM to find the trained parameter is only 0.0313 second. In addition, from Fig. 8 it is found that the maximum error for K_p is 0.0268 and the minimum error is 0.0232. Furthermore, the MSE value for K_p is 0.0232. It was also noticeable that from Fig. 9 that the maximum error for K_i value is 0.0097 while the minimum error for K_i value is 0.0083. In addition, the MSE value for K_i is 0.00898. From these results it can be concluded that, the ELM can predict the PI parameter based on the operating condition.

4.2. Testing phase

The second case study is the testing phase. After the PI controller is trained with the ELM, the next step is to test the PI controller under different speed reference. In this section the throttle of the electric vehicle is set to have rotation from 0 to 157 rpm. The

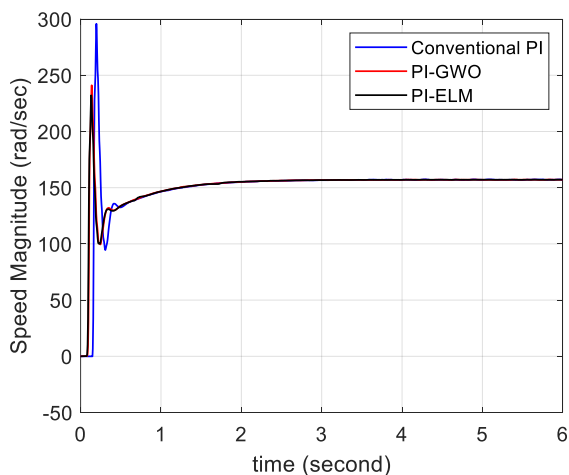


Figure. 10 Comparison of electric vehicle speed response under different scenarios

Tabel 5. Detailed features of Fig. 7

Parameter	PI-ELM	PI GWO	PI Conventional
Overshoot (rpm)	221.6	240.3	295.45
Settling time (second)	3.8	4.6	5

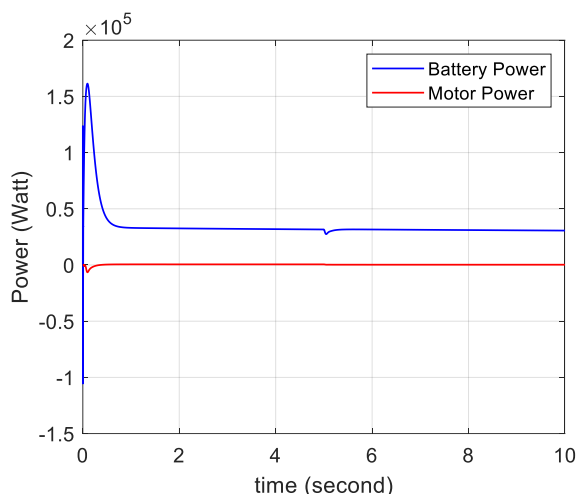


Figure. 11 Comparison of battery and motor power under regenerative braking conditions

Tabel 6. Execution time comparison

Remark	PI-ELM	PI GWO
Execution time (second)	0.0313	256

load torque is neglected in this testing section. Two different scenarios are considered to investigate the efficacy of the proposed method. The first scenario is system with conventional PI. The second scenario is system with adaptive PI based on ELM (black line) and the third scenario is system with PI controller based on GWO (red line). Fig. 10 shows the electric vehicle speed response under 157 speed

reference. In addition, Table 5 shows the detailed features of Fig. 7.

From Fig. 10 and Table 5 it is observed that when PI is designed adaptive using ELM, they can give more better signal controller than using conventional PI. This is indicated by the speed response of the electric vehicle. It is noticeable that the speed response of system with PI based ELM have smaller overshoot and fastest settling time than system using conventional PI controller. This could be happening because PI based ELM give better control signal to the duty cycle so that the bidirectional converter is giving better voltage input to the electric vehicle.

For further investigation, the comparison of execution time between PI based on ELM and PI based on GWO is essential. Table 6 shows the execution time comparison between PI based on ELM (proposed method) and PI based on GWO. It is found that the execution time of PI based ELM is faster that execution time of PI based GWO. The execution time is expected to increase as the system's size and complexity grow. As a results, it is important to use a method with shorter execution time.

4.3 Regenerative braking conditions

In this section, the system is tested against regenerative braking conditions. To simulate regenerative braking first the load torque is set to have 180 Nm value. Then the load torque is reduced to become 90 Nm. In addition, the speed reference is also reduced from 157 to 127 rpm. It should be noted that in this case only the proposed method scenario is used to test the regenerative braking condition. Fig. 11 shows the comparison between electric vehicle power and battery power.

When braking conditions occur on the motor, the load torque will be negative, and the motor will change its function to a generator. The motor that has switched the function will supply power to the battery. This causes the process of charging the battery. Referring to the curve in Figure. 12, the battery input power response reaches a steady state condition at 5 seconds. The value of the battery input power ranges from ± 31.64 kW at steady state conditions. The time required for the motor output power response to steady state is 5 seconds. In steady state condition, the motor output power is ± 2.79 kW.

5. Conclusions

This paper focused on designing bidirectional converter controller using ELM. The purpose of using ELM is to make the converter controller adaptive to any changing on the operating condition. The PI controller is used as the bidirectional

converter controller. From the simulation results it is found that the ELM can mimic the actual parameter of conventional PI. For both parameter the MSE value is less than 0.03 for K_p and 0.01 for K_i . In addition, the PI based on ELM is giving better controller response than conventional PI. This is indicated by the speed response of electric vehicle. The speed response of the system with PI-ELM has less overshoot than system with conventional PI controller. Furthermore, in the regenerative braking condition the PI based ELM is giving better results than system using conventional controller.

Conflicts of interest

“The authors declare no conflict of interest.”

Author contributions

“Conceptualization, Herlambang Setiadi, Yusrizal Afif; methodology, Herlambang Setiadi, Muhammad Abdillah; validation, Herlambang Setiadi, Yusrizal Afif; format analysis, Yusrizal Afif, Muhammad Abdillah and Herlambang Setiadi; investigation, Herlambang Setiadi, Yusrizal Afif; resources, Herlambang Setiadi; writing original draft preparation, Herlambang Setiadi; writing review and editing Herlambang Setiadi, Yusrizal Afif, Muhammad Abdillah; visualization, Herlambang Setiadi, Yusrizal Afif. All authors have read and agreed to the published version of the manuscript”.

References

- [1] H. Setiadi, N. Mithulananthan, and R. Shah, “Design of wide-area POD with resiliency using modified DEA for power systems with high penetration of renewable energy”, *IET Renewable Power Generation*, Vol. 13, No. 2, pp. 342–351, 2018.
- [2] A. U. Krismanto, N. Mithulananthan, H. Setiadi, E. Y. Setyawan, and M. Abdillah, “Impacts of grid-tied microgrid on stability and interaction of power systems considering RE uncertainties”, *Sustainable Energy, Grids and Networks*, Vol. 28, p. 100537, 2021.
- [3] R. Hou, L. Lei, K. Jin, X. Lin, and L. Xiao, “Introducing electric vehicles? Impact of network effect on profits and social welfare”, *Energy*, Vol. 243, p. 123002, 2022.
- [4] K. Hamza, K. C. Chu, and K. Laberteaux, “A Study on the Impact of Driving in Charge Mode on Well-To-Wheels Greenhouse Gas Emissions of Plug-in Hybrid Electric Vehicles”, *SAE Technical Paper*, 2022.
- [5] E. Kazemzadeh, M. Koengkan, and J. A. Fuinhas, “Effect of Battery-Electric and Plug-In Hybrid Electric Vehicles on PM_{2.5} Emissions in 29 European Countries”, *Sustainability*, Vol. 14, No. 4, p. 2188, 2022.
- [6] M. Vilaça, G. Santos, M. S. A. Oliveira, M. C. Coelho, and G. H. A. Correia, “Life cycle assessment of shared and private use of automated and electric vehicles on interurban mobility”, *Applied Energy*, Vol. 310, p. 118589, 2022.
- [7] M. Karthik, S. Usha, K. Venkateswaran, H. Panchal, M. Suresh, V. Priya, and K. K. Hinduja, “Evaluation of electromagnetic intrusion in brushless DC motor drive for electric vehicle applications with manifestation of mitigating the electromagnetic interference,” *International Journal of Ambient Energy*, pp. 1–8, 2020.
- [8] S. Arof, N. H. N. Diyanah, N. M. Noor, J. A. Jalil, P. A. Mawby, and H. Arof, “A new four quadrants drive chopper for separately excited DC motor in low-cost electric vehicle”, *Progress in Engineering Technology*, pp. 119–138, 2019.
- [9] C. Huang, F. Lei, X. Han, and Z. Zhang, “Determination of modeling parameters for a brushless DC motor that satisfies the power performance of an electric vehicle”, *Measurement and Control*, Vol. 52, No. 7–8, pp. 765–774, 2019.
- [10] M. Bahrami, H. Mokhtari, and A. Dindar, “Energy regeneration technique for electric vehicles driven by a brushless DC motor”, *IET Power Electronics*, Vol. 12, No. 13, pp. 3397–3402, 2019.
- [11] K. S. Kavin and P. S. Karuvelam, “PV-based Grid Interactive PMBLDC Electric Vehicle with High Gain Interleaved DC-DC SEPIC Converter”, *IETE Journal of Research*, pp. 1–15, 2021.
- [12] S. Chakraborty, M. M. Hasan, P. McGahan, D. T. Duong, T. Geury, P. Davari, F. Blaabjerg, M. E. Baghdadi, and O. Hegazy, “Real-Life Mission Profile Oriented Lifetime Estimation of a SiC Interleaved Bidirectional HV DC/DC Converter for Electric Vehicle Drivetrains”, *IEEE Journal of Emerging and Selected Topics in Power Electronics*, 2022.
- [13] C. G. Castaño, C. Restrepo, S. Kouro, E. V. Idiarte, and J. Calvente, “A Bidirectional Versatile Buck–Boost Converter Driver for Electric Vehicle Applications”, *Sensors*, Vol. 21, No. 17, p. 5712, 2021.
- [14] M. Kumar, K. Chaudhary, R. K. Saket, and B. Khan, “Bidirectional Quadratic Converter-Based PMBLDC Motor Drive for LEV Application”, *Journal of Electrical and Computer Engineering*, Vol. 2022, 2022.

- [15] Z. U. Haq and A. Ali, "Comparative study of Zeta converter and Boost converter Using PI controller", In: *Proc. of 2021 7th International Conference on Electrical, Electronics and Information Engineering (ICEEIE)*, pp. 54–59, 2021.
- [16] S. Gurung, F. Jurado, S. Naetiladdanon, and A. Sangswang, "Comparative analysis of probabilistic and deterministic approach to tune the power system stabilizers using the directional bat algorithm to improve system small-signal stability", *Electric Power Systems Research*, Vol. 181, p. 106176, 2020.
- [17] A. M. Allam, A. S. Ibrahim, and E. Nabil, "Single loop PID controller design based on optimization algorithms for parallelly connected dc-dc converters", *Journal of Physics: Conference Series*, Vol. 2128, No. 1, p. 012027, 2021.
- [18] J. Á. León, C. D. C. Palacios, C. V. Salgado, E. H. Perez, and E. X. M. García, "Optimal PID Parameters Tuning for a DC-DC Boost Converter: A Performance Comparative Using Grey Wolf Optimizer, Particle Swarm Optimization and Genetic Algorithms", In: *Proc. of 2020 IEEE Conference on Technologies for Sustainability (SusTech)*, pp. 1–6, 2020.
- [19] M. Abdillah and H. Setiadi, "Advanced Wide-Area Monitoring System Design for Electrical Power System", *International Review on Modelling and Simulations (IREMOS)*, Vol. 13, No. 6, Dec. 2020, [Online]. Available: <https://www.praiseworthyprize.org/jsm/index.php?journal=iremos&>
- [20] C. Rim, G. B. Joung, and G. H. Cho, "A state space modeling of non-ideal DC-DC converters", In: *Proc. of PESC 88 Record 19th Annual IEEE Power Electronics Specialists Conference*, pp. 943–950, 1988.
- [21] P. Andre, "Konverter Nonisolated Bidirectional DC Berbasis Coupled Inductor Untuk Aplikasi Kendaraan Listrik", *Institut Teknologi Sepuluh Nopember*, Surabaya, 2013.
- [22] A. Sharma, S. S. Nag, G. Bhuvaneswari, and M. Veerachary, "An improved mode transition technique for a non-isolated bidirectional DC-DC converter", *IEEE Transactions on Circuits and Systems II: Express Briefs*, Vol. 67, No. 12, pp. 3093–3097, 2020.
- [23] S. Fan, H. He, S. Chen, J. Duan, J. You, and L. Bai, "Zero voltage switching non-isolated bidirectional DC-DC converter with transient current built-up technique", *Journal of Power Electronics*, pp. 1–9, 2022.
- [24] S. O. D. Luiz, E. G. Souza, and A. Lima, "Representing the Accumulator Ageing in an Automotive Lead-Acid Battery Model", *Journal of Control, Automation and Electrical Systems*, Vol. 33, No. 1, pp. 204–218, 2022.
- [25] B. Liu, G. Chen, H. C. Lin, W. Zhang, and J. Liu, "Prediction of IGBT junction temperature using improved cuckoo search-based extreme learning machine", *Microelectronics Reliability*, Vol. 124, p. 114267, 2021, doi: <https://doi.org/10.1016/j.microrel.2021.114267>.
- [26] I. B. G. Manuaba, M. Abdillah, R. Zamora, and H. Setiadi, "Adaptive Power System Stabilizer Using Kernel Extreme Learning Machine", *International Journal of Intelligent Engineering and Systems*, Vol. 14, No. 3, pp. 468-480, 2021, doi: 10.22266/ijies2021.0630.39.
- [27] P. Pi and D. Lima, "Gray level co-occurrence matrix and extreme learning machine for Covid-19 diagnosis", *International Journal of Cognitive Computing in Engineering*, Vol. 2, pp. 93–103, 2021, doi: <https://doi.org/10.1016/j.ijcce.2021.05.001>.
- [28] H. Setiadi, R. Shah, M. R. Islam, D. A. Asfani, T. H. Nasution, M. Abdillah, P. Megantoro, and A. U. Krismanto, "An Extreme Learning Machine Based Adaptive VISMA for Stability Enhancement of Renewable Rich Power Systems", *Electronics (Basel)*, Vol. 11, No. 2, p. 247, 2022.